

A novel autoregulatory loop between the Gcn2-Atf4 pathway and L-Proline metabolism controls stem cell identity

This article has been corrected since Advance Online Publication and an erratum is also printed in this issue

C D'Aniello^{1,4}, A Fico^{1,4}, L Casalino¹, O Guardiola¹, G Di Napoli¹, F Cermola¹, D De Cesare¹, R Tatè², G Cobellis³, EJ Patriarca^{*1} and G Minchiotti^{*1}

Increasing evidence indicates that metabolism is implicated in the control of stem cell identity. Here, we demonstrate that embryonic stem cell (ESC) behaviour relies on a feedback loop that involves the non-essential amino acid L-Proline (L-Pro) in the modulation of the Gcn2-Eif2 α -Atf4 amino acid starvation response (AAR) pathway that in turn regulates L-Pro biosynthesis. This regulatory loop generates a highly specific intrinsic shortage of L-Pro that restricts proliferation of tightly packed domed-like ESC colonies and safeguards ESC identity. Indeed, alleviation of this nutrient stress condition by exogenously provided L-Pro induces proliferation and modifies the ESC phenotypic and molecular identity towards that of mesenchymal-like, invasive pluripotent stem cells. Either pharmacological inhibition of the prolyl-tRNA synthetase by halofuginone or forced expression of Atf4 antagonises the effects of exogenous L-Pro. Our data provide unprecedented evidence that L-Pro metabolism and the nutrient stress response are functionally integrated to maintain ESC identity.

Cell Death and Differentiation (2015) 22, 1094–1105; doi:10.1038/cdd.2015.24; published online 10 April 2015

Naturally occurring amino acids are emerging as key players in the regulation of the phenotypic plasticity of stem cells.^{1–5} Indeed, exogenously provided threonine and methionine, two essential amino acids (EAAs), regulate self-renewal and differentiation of pluripotent stem cells.² Moreover, exogenously provided L-Proline (L-Pro), a non-essential amino acid (NEAA), induces mouse ESCs towards an embryonic stem cell-to-mesenchymal-like transition (esMT) that converts compact, adherent ESCs into mesenchymal-like spindle-shaped, highly invasive and metastatic pluripotent stem cells.⁴ This fully reversible process resembles the epithelial-to-mesenchymal transition (EMT), which is essential for normal development and contributes to pathological cancer progression.^{6–8} Interestingly, the *Aldh18a1* gene is specifically induced in and marks the Primitive Endoderm (PrE) in the time window when the pluripotent epiblast precursors are specified within the inner cell mass (ICM) of the blastocyst.⁹ Since the *Aldh18a1* enzyme catalyses the first and rate-limiting step of L-Pro biosynthesis, these findings suggest that L-Pro metabolism may regulate cell lineage segregation in early mammalian embryos. Despite its relevance, the molecular mechanisms underlying L-Pro control of stem cell identity remain largely unknown. This prompted us to investigate the early molecular events regulated by exogenously provided L-Pro in mouse ESCs.

Results

L-Pro modulates the AAR pathway. To provide insights into the earliest molecular events of L-Pro-induced embryonic stem cell-to-mesenchymal-like transition (esMT), we first analysed the transcriptome of ESCs grown at low density under feeder-free condition, at 24 and 48 h +/- L-Pro, in DMEM/FBS/LIF complete medium. Approximately 250 protein-coding genes were deregulated by L-Pro at 24 h (≥ 1.5 -fold-change, $fdr < 0.0001$), and this increased to approximately 900 genes at 48 h (Figures 1a and b; Supplementary Table 1). Gene ontology analysis revealed enrichment in genes involved in amino-acid metabolism at 24 h and in genes involved in focal adhesion and TGF β signalling at 48 h (Figure 1c). Notably, the mesenchymal-like features became evident only later on, that is, at day 3 of the esMT.⁴ Among the genes early downregulated after L-Pro addition (Supplementary Table 1), we focused our attention on the stress-activated transcription factor 4 (Atf4). Interestingly, 77% (14/18) of the genes inhibited by L-Pro (≥ 2 -fold change at 24 h) (Supplementary Table 1) are direct targets of Atf4.¹⁰ Atf4 is the main downstream effector of an evolutionarily conserved stress pathway known as the amino acid starvation response (AAR) (Figure 1d), which is induced by uncharged tRNAs that bind to and activate the general

¹Institute of Genetics and Biophysics 'A. Buzzati-Traverso', CNR, Naples, Italy; ²Integrated Microscopy, Institute of Genetics and Biophysics 'A. Buzzati-Traverso', CNR, Naples, Italy and ³Department of Biophysics, Biochemistry and General Pathology, Second University of Naples (SUN), Naples, Italy

*Corresponding author: EJ Patriarca or G Minchiotti, Stem Cell Fate Laboratory, Institute of Genetics and Biophysics, Via Pietro Castellino 111, Naples 80131, Italy. Tel: +39 816132357; Fax: +39 816132706; E-mail: gabriella.minchiotti@igb.cnr.it or eduardo.patriarca@igb.cnr.it

⁴These authors contributed equally to this work.

Abbreviations: AAR, amino-acid starvation response pathway; Atf4, stress-activated transcription factor 4; EAAs, essential amino acids; NEAAs, nonessential amino acids; ESCs, embryonic stem cells; esMT, embryonic stem cell-to-mesenchymal-like transition; Eif2 α , eukaryotic initiation factor 2; Gcn2, general control nonrepressed 2 protein kinase; HF, halofuginone; L-His, Histidine; ICM, inner cell mass; LC3, microtubule-associated protein light chain 3; L-Pro, L-Proline; PiCs, proline-induced cells; PRS, prolyl-tRNA synthetase

Received 30.7.14; revised 07.2.15; accepted 16.2.15; Edited by N Chandel; published online 10.4.15

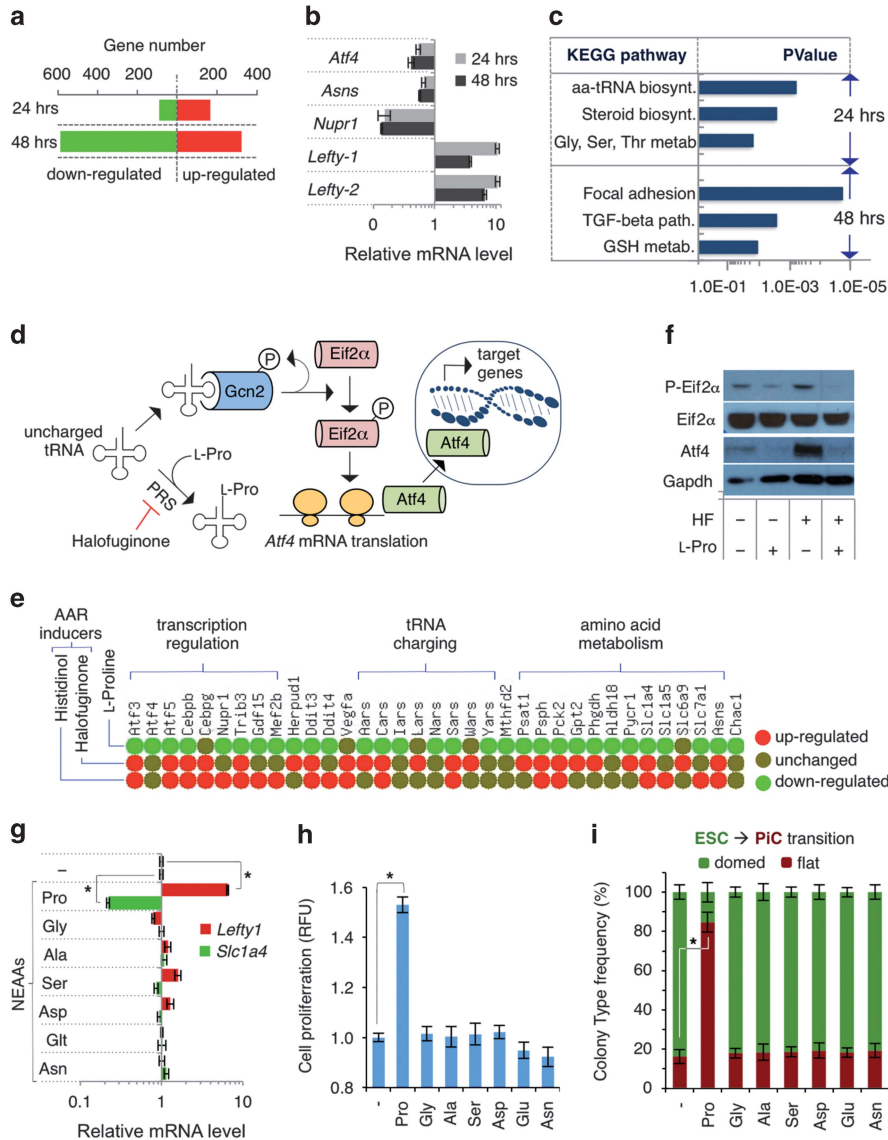


Figure 1 L-Pro rapidly remodels the ESC transcriptome and modulates the AAR pathway. (a) Genes deregulated (≥ 1.5 -fold; $FDR < 0.0001$) by L-Pro (0.5 mM) in TBV2 ESCs at 24 and 48 h, as inferred from microarray analysis (Supplementary Table 1). (b) Time course of qPCR analysis of selected genes in L-Pro-treated versus untreated ESCs. Data are presented as fold change compared with control after normalisation to *Gapdh*. (c) Gene ontology (GO) analysis of L-Pro-treated ESC transcriptome showing gene enrichment in KEGG pathway. (d) Schematic representation of the AAR (Gcn2-Eif2 α -ATF4) pathway. (e) Heat-map diagram showing AAR-related genes downregulated (green) in L-Pro-treated ESCs or upregulated (red) by histidinol (HisOH) and halofuginone (HF). (f) Western blot analysis of phospho-(⁵¹Ser)-Eif2 α and Atf4 in ESCs treated (8 h) with L-Pro (0.5 mM) or HF (8 nM) either alone or in combination. *Gapdh* was used as a loading control. (g) Effects of different NEAAs on the expression of AAR-related and AAR-unrelated genes. qPCR analysis of *Lefty1* and *Slc1a4* in ESCs treated with individual NEAA (0.5 mM) or left untreated as a control (24 h). (h) Effects of different NEAAs on ESC proliferation (36 h). Proliferation was measured by the CyQuant[®] assay and expressed as relative fluorescence units (RFU). (i) Effect of different NEAAs on the ESC to PIC transition. Colony-type frequency (domed versus flat) of ESCs +/- individual NEAA as assessed (~300 colonies scored/condition) at day 5 after plating. See Supplementary Figure 1. Data represent the mean \pm S.D. from (b, f, g and i) three or (h) five independent experiments, * $P < 0.001$

control nonrepressed 2 (Gcn2) protein kinase, leading to phosphorylation of the eukaryotic initiation factor 2 (Eif2 α) and to translation of *Atf4* mRNA.^{11,12} Accordingly, L-Pro downregulated a set of AAR/Atf4-related genes¹³ involved in non-essential amino acid (NEAA) biosynthesis, amino-acid transport or tRNA loading (Figure 1e). Remarkably, a similar set of genes was found to be upregulated in human T helper (T_H17) cells treated with halofuginone (HF) (Figure 1e), a low-molecular weight alkaloid that induces L-Pro starvation by selectively inhibiting prolyl-tRNA synthetase (PRS).^{14,15}

Consistent with these findings, L-Pro and HF induced opposite effects on Eif2 α phosphorylation and Atf4 protein levels (Figure 1f) and, remarkably, the effect of HF activity was fully counterbalanced by supplemental L-Pro (Figure 1f), suggesting that L-Pro availability regulates AAR in ESCs. We then assessed the specificity of L-Pro and showed that none of the NEAA other than L-Pro either reduced the expression of AAR markers (Figure 1g; Supplementary Figure 1a) or induced TGF β -related genes (*Lefty1*, *Lefty2*) (Figure 1g; Supplementary Figure 1b). Moreover, none of them

induced ESC proliferation (Figure 1h) or the ESC to PiC phenotypic transition (esMT) (Figure 1i; Supplementary Figure 1c). Finally, as expected by the fact that EEAs are already present in the culture medium, a further addition of essential amino acids (EEAs), either as a mix or individually, did not induce ESC proliferation (data not shown). We thus concluded that L-Pro is the unique growth-limiting amino acid for ESCs cultured in complete medium (DMEM/FBS/LIF).

It is known that mitochondrial L-Pro catabolism generates reactive oxygen species (ROS), which, in turn, could activate redox-sensitive signalling pathways.^{16,17} We thus evaluated the effect of increasing concentrations of two antioxidants, N-Acetyl-Cysteine (NAC) and Glutathione (GSH) on L-Pro induced ESC proliferation and AAR inactivation. Neither NAC nor GSH counteracted L-Pro activity (Supplementary Figures 1d and e), even at the highest concentration (5 mM) thus ruling out the possibility that L-Pro induced ESC proliferation and AAR inactivation correlate with ROS accumulation.

Finally, we measured the intracellular concentration of free L-Pro and found that it was ~4-fold lower in ESCs compared with PiCs, which in turn was ~10-fold lower than in mouse embryonic fibroblasts (MEFs) (Supplementary Figure 1f). All together, our results indicate that ESCs grown in complete medium experience an intrinsic and specific L-Pro shortage (nutritional stress) that activates AAR, limits their proliferation and prevents the esMT, and that this stress is alleviated by exogenously provided L-Pro.

Halofuginone antagonises L-Pro-induced proliferation and EsMT. We have shown that HF prevented L-Pro-dependent AAR inactivation (Figure 1f). We therefore hypothesised that if L-Pro-induced ESC proliferation and esMT relied on AAR neutralization, HF should prevent both effects. Accordingly, HF (6–10 nM) antagonised the pro-proliferative effect of L-Pro (0.2–0.5 mM) in a dose-dependent manner (Figure 2a). In the absence of L-Pro, 2 nM HF inhibited ESC proliferation (Figure 2a). Consistent with this, HF also prevented L-Pro-induced downregulation of AAR-specific markers (Figure 2b; Supplementary Figure 2a). We then assessed the effect of Cycloheximide and Histidinol, which block protein synthesis by different mechanisms. Both inhibitors reduced ESC proliferation and induced AAR-specific markers in a dose-dependent manner (Supplementary Figures 2b and c). However, while exogenously added L-Pro fully counterbalanced the effect of HF (Figure 2c), it failed to antagonise the effect of Cycloheximide and Histidinol on both ESC proliferation and modulation of AAR-specific markers (Supplementary Figures 2b and c). Notably, none of the other NEAA neutralised the anti-proliferative effect of HF (Figure 2c), indicating that HF maintains a high specificity for PRS in ESCs. In particular, neither L-Glutamate (L-Glu) nor L-Ornithine (L-Orn), two different metabolic precursors of L-Pro biosynthesis, was able to efficiently counteract the anti-proliferative effect of HF (Figure 2c; Supplementary Figure 2d); thus supporting the idea that L-Pro biosynthesis from L-Glu or L-Orn does not efficiently occur in ESCs.

Finally, we found that the NEAA mix partially counteracted HF (Figure 2c), probably because L-Gly, L-Ser and L-Ala

compete with L-Pro for the same transporter, reducing its uptake.^{1,18}

We thus went on to evaluate the effect of HF on the L-Pro-induced esMT. Consistent with competitive inhibition of PRS activity, HF neutralised the esMT in a dose-dependent manner (Figures 2d–f; Supplementary Figures 2e and f). HF prevented the induction of PiC markers (*Fgf5*, *Brachyury*, *Pitx2*) (Figure 2g) and the acquisition of a motile phenotype (Supplementary Figure 2g). Moreover, L-Pro/HF-treated ESCs developed Alkaline Phosphatase-positive (AP+) domed colonies (Figure 2h) and efficiently differentiated *in vitro* both in cardiomyocytes and in neurons (Figures 2i and j). Finally, HF reverted the esMT inducing the PiC to ESC phenotypic transition, even in the presence of supplemental L-Pro (Supplementary Figure 2h). We thus concluded that HF counteracted L-Pro effects without affecting ESC pluripotency and suggest that the esMT relies on AAR neutralisation.

L-Pro and AAR are mutually regulated defining a novel autoregulatory loop. To develop mechanistic insights, we first generated and characterised *shRNA*-mediated *Atf4* knockdown (KD) ESCs (≥80% silencing) (Supplementary Figures 3a and c). *Atf4* KD downregulated AAR but not pluripotency-related genes (Supplementary Figure 3d), and it reduced ESC proliferation in the absence of L-Pro (Figure 3a), as described in amino acid-starved cells.¹³ Nevertheless, L-Pro, but none of the other NEAA, induced the proliferation of control and *Atf4* KD cells at comparable levels (Figures 3a and b). We then evaluated the response of *Atf4* KD ESCs to HF (Figure 3c) and found that *Atf4* KD increased the susceptibility of ESCs to HF, even when added at sub-lethal concentrations (1–2 nM) (Figure 3d). Most remarkably, L-Pro fully antagonised HF, inducing the proliferation of control and *Atf4* KD ESCs at comparable levels (Figure 3d). Furthermore, *Atf4* KD ESCs developed significantly smaller (approximately half the size) colonies compared with controls (Figures 3e and f; Supplementary Figure 3e). Thus, *Atf4* is required to improve ESC proliferation/survival. We evaluated whether *Atf4* downregulation could affect the esMT. Indeed, similar to the control, *Atf4* KD ESCs developed flat colonies only in the presence of L-Pro (Figure 3e), indicating that *Atf4* downregulation *per se* is not sufficient to induce the ESC to PiC transition. We then used a complementary gain-of-function (GOF) approach based on the ROSA-TET-OFF system¹⁹ to assess the effect of *Atf4* overexpression. As expected, *Atf4* overexpression (Figure 3g; Supplementary Figure 3f) upregulated AAR but not pluripotency markers (Supplementary Figure 3g), and it eventually induced ESC proliferation/survival (Figure 3h; Supplementary Figure 3h), thus leading to the formation of larger colonies even in the absence of supplemental L-Pro (Figure 3i; Supplementary Figure 3i). Remarkably, in the presence of L-Pro, *Atf4* GOF ESCs (–Tet) developed domed, compacted colonies lacking the typical crown of mesenchymal-like cells scattered around the colony core of (–Tet) control cells (Figure 3i; Supplementary Figure 3i). Accordingly, cell motility was impaired in *Atf4* GOF cells (Figure 3j). We thus concluded that L-Pro-mediated AAR inactivation/*Atf4* downregulation is crucial for the acquisition of the mesenchymal-like motile phenotype.

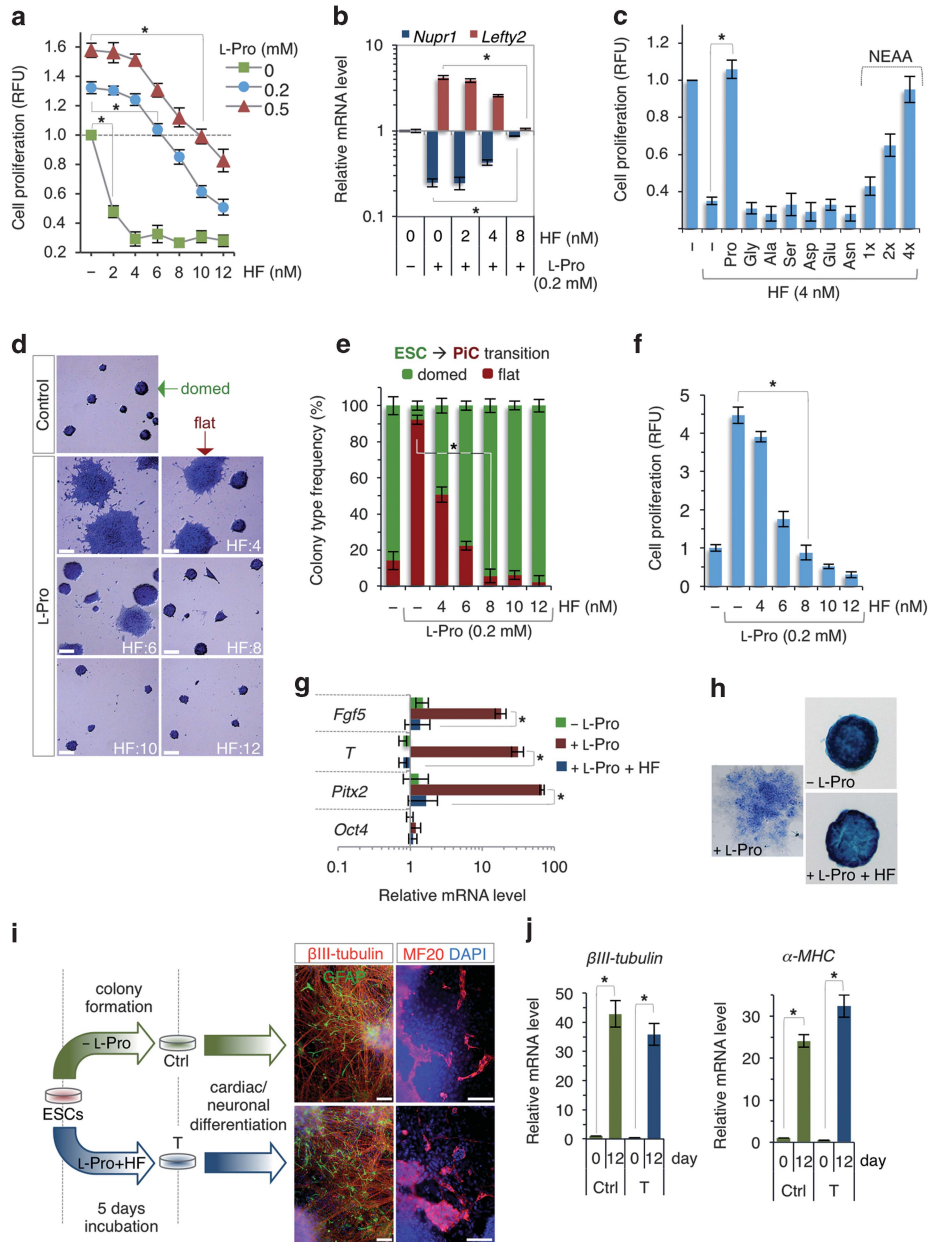


Figure 2 Halofuginone antagonises L-Pro-induced ESC proliferation and esMT. (a and b) Dose-dependent effect of HF on ESC proliferation and molecular markers' expression. Proliferation of ESCs treated (L-Pro +/- HF) or untreated (control) was measured at 36 h after plating by CyQuant[®] assay and expressed as Relative Fluorescence Intensity (RFU). The mRNA level of *Nupr1* and *Lefty2* genes (b) was assayed by qPCR at 24 h after plating. (c) Only L-Pro among NEAAs counteracts the anti-proliferative effect of HF. ESC proliferation was measured at 36 h after the addition of either individual (0.2 mM) or mixed (0.1 mM/each) NEAAs. (d–f) Effect of HF on L-Pro-induced esMT. Representative photomicrographs (d) of colonies generated from ESCs +/- L-Pro (0.2 mM) alone or with HF and stained with crystal violet at day 5. Scale bar, 75 μ m. Colony phenotype frequency (e) at day 5 after plating (domed versus flat) (300 colonies scored/condition). Cell proliferation (f) was measured by CyQuant[®] assay and expressed as RFU. (g) qPCR analysis of PiC markers *Fgf5*, *T* and *Pitx2* and of the pluripotency marker *Oct4* in ESCs treated with L-Pro +/- HF. (h) Colonies positive for alkaline phosphatase derived from control (-L-Pro), L-Pro (0.2 mM) and L-Pro (0.2 mM)/HF (8 nM)-treated ESCs at day 5 after plating. (i) Schematic representation of the experimental procedure. Colonies derived from control (-L-Pro) and L-Pro (0.2 mM)/HF (8 nM) treated ESCs at day 5 after plating, were induced to either neural or cardiac differentiation. Immunofluorescence analysis of neuronal (left) and cardiac (right) differentiation of the control and L-Pro/HF-treated ESCs, showing large areas of cells positive for β -III tubulin, GFAP and α -myosin heavy chain (α -MHC), respectively. The nuclei were visualised with DAPI (blue). Scale bar, 75 μ m. (j) qPCR analysis of neuronal (β -III tubulin) and cardiac (α -MHC) specific markers in control (Ctrl, green) and L-Pro/HF-treated (T, blue) ESCs. Data represent the mean \pm SD from three (b, c, e, f, g and j) or five (a) independent experiments, * P < 0.001

The opposing effects of *Atf4* KD and GOF on ESC proliferation correlate well with the positive control of *Atf4* on L-Pro biosynthesis. In mammalian cells, L-Pro is synthesised from L-Glu by a reductive process involving two enzymes,

pyrroline-5-carboxylate synthetase and pyrroline-5-carboxylate reductase, encoded by *Aldh18a1* and *Pycr1*, respectively. Indeed, both these genes were early downregulated after L-Pro addition (Figure 1e). Furthermore, HF induced

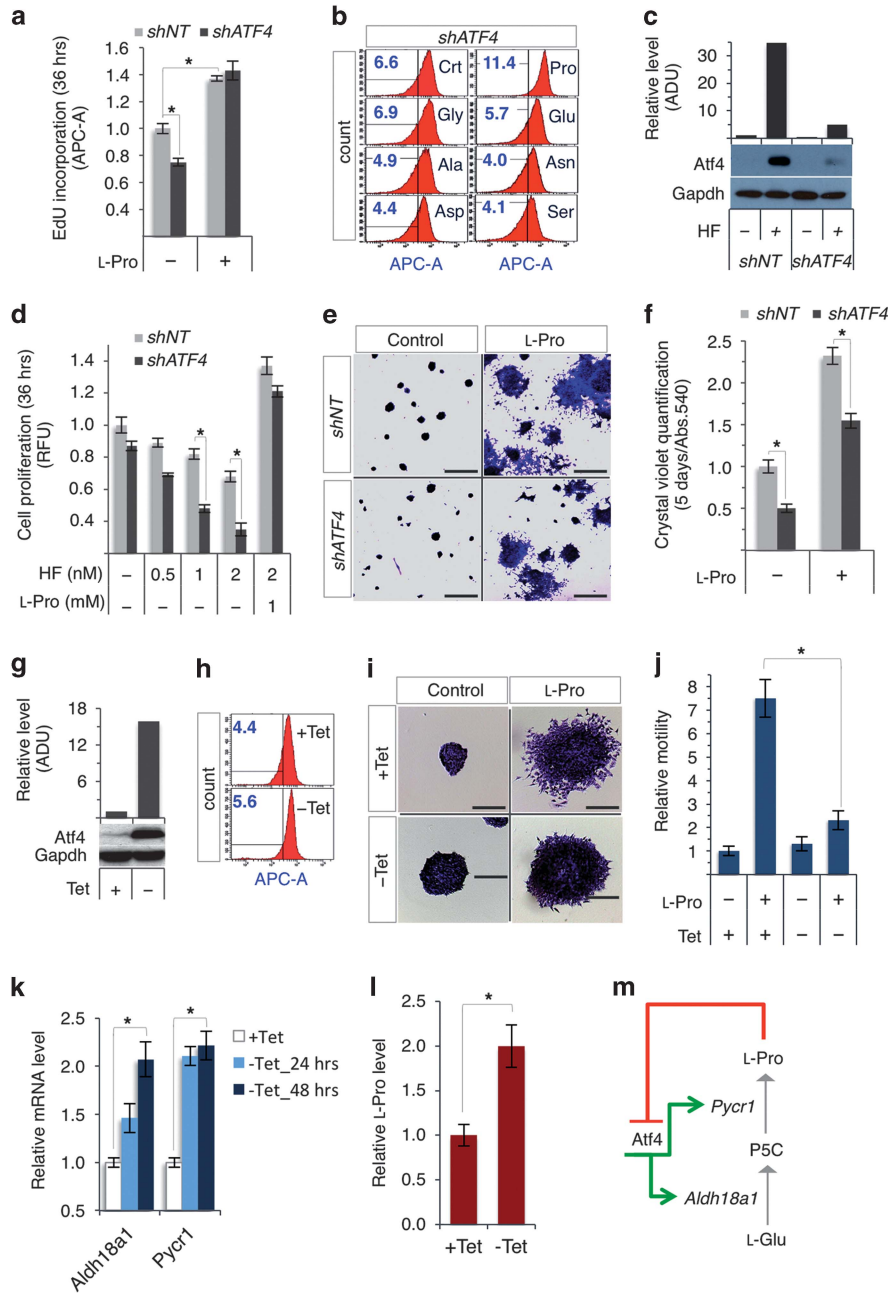


Figure 3 Biological effects of L-Pro-dependent modulation of the AAR pathway in ESCs. (**a** and **b**) Effect of *Atf4* KD on ESC proliferation. FACS-based analysis (EdU incorporation) of *Atf4* KD (*shATF4*) and control (*shNT*) ESCs proliferation (**a**) performed at 36 h after plating. The results are expressed as the fold change compared with control. Representative FACS plots of EdU incorporation (**b**) in *Atf4* KD ESC +/- individual NEAAs (0.5 mM) at 36 h after plating. (**c**) Western blot analysis of *Atf4* in untreated or HF-treated *Atf4* KD and control ESCs (36 h). The densitometric analysis is expressed in ADU as the *Atf4*/Gapdh ratio. (**d**) Proliferation of control and *Atf4* KD ESCs after 48 h treatment with HF, either alone or with L-Pro, was measured by CyQuant[®] and expressed as RFU. (**e** and **f**) Effect of *Atf4* KD on cell colony formation. Representative photomicrographs (**e**) of colonies generated from *Atf4* KD and control ESCs plated +/- L-Pro (0.2 mM) and stained with crystal violet at day 5. Scale bar, 200 μ m. Quantification of crystal violet staining of cell colonies generated in the different culture conditions (**f**). (**g**–**j**) Effect of *Atf4* overexpression on ESCs behaviour. Immunoblotting analysis of *Atf4* protein (**g**) in *Atf4* Tet-OFF ESCs +/- Tet at 48 h. The densitometric analysis is expressed in ADU as the *Atf4*/Gapdh ratio. Representative FACS plots of EdU incorporation (**h**) in *Atf4* Tet-OFF ESCs +/- Tet. Representative photomicrographs of colonies (**i**) generated from *Atf4* Tet-OFF ESCs treated with +/- Tet and +/- L-Pro (0.2 mM) and stained with crystal violet at day 5 after plating. Scale bar, 50 μ m. Effect of *Atf4* overexpression on L-Pro-induced cell motility (**j**). Control (+Tet) and *Atf4* GOF (-Tet) ESCs were treated with +/- L-Pro and migration was assessed at day 5 after plating. The results show the average numbers of cells migrating towards an FBS gradient (1–15%). (**k**) qPCR analysis of *Aldh18a1* and *Pycr1* in control (+Tet) and *Atf4* GOF (-Tet) at 24 h and 48 h. (**l**) The intracellular free L-Pro concentration was measured in control (+Tet) and *Atf4* GOF (-Tet) ESCs at day 5 after plating. The results are expressed as the fold change compared with control. (**m**) Schematic representation of the L-Pro-AAR/Atf4 regulatory feedback loop. Data represent the mean \pm S.D. from (**a**, **b**, **c**, **f**, **g**, **h**, **j**, **k**, and **l**) three or (**d**) five independent experiments, * $P < 0.001$

Aldh18a1 and *Pycr1* expression, and this effect was fully counteracted by L-Pro (Supplementary Figure 3j). Finally, *Aldh18a1* and *Pycr1* were upregulated in *Atf4* GOF (Figure 3k), and the intracellular level of free L-Pro consequently increased (Figure 3l). These data are in line with previous findings that *Atf4* directly binds to the promoter region of *Aldh18a1* gene¹⁰ and that *Pycr1* expression depends on AAR/*Atf4* pathway.²⁰

Therefore, our findings identify a novel regulatory feedback loop (Figure 3m) in which L-Pro modulates AAR activity/*Atf4* expression, which in turn regulates L-Pro biosynthesis (*Aldh18a1* and *Pycr1* expression), thus explaining the maintenance of the specific intrinsic shortage of L-Pro in ESCs.

L-Pro starvation induces autophagy in ESCs. In mammals, amino-acid starvation induces autophagy, a mechanism by which the cells digest their own proteins and organelles.^{21,22} Because ESCs are starved of L-Pro, we evaluated autophagy induction. We first analysed the intracellular distribution of the microtubule-associated protein light chain 3 (LC3), which shifts from diffuse to punctate during autophagosome formation.²³ ESCs stably expressing either a GFP-LC3 wild-type fusion (LC3_wt) or a control GFP-LC3G120A mutant (LC3_mut) that fails to localise to autophagosomes²⁴ were generated and propagated on feeder MEFs. When plated on gelatin-coated plates without L-Pro, LC3_mut cells maintained a diffuse GFP distribution, whereas LC3_wt ESCs showed punctate GFP-LC3 foci, which markedly increased with time (Figure 4a; Supplementary Figure 4a). Remarkably, L-Pro prevented LC3-GFP puncta formation specifically and in a dose-dependent manner (Figures 4b and c; Supplementary Figure 4b). HF fully counteracted L-Pro and further increased the percentage of cells with punctate LC3-GFP expression (Figure 4d). Our findings suggest that L-Pro starvation, either intrinsic or pharmacologically induced by HF, activates autophagy in ESCs. To evaluate whether L-Pro starvation resembles that of EAA, we used the Histidinol that mimics Histidine starvation and induces autophagy.²⁵ Interestingly, Histidinol increased the percentage of ESCs with punctate LC3-GFP signal (Supplementary Figure 4c and d), thus indicating that L-Pro starvation in ESCs resembles that of EAA, and exerts similar effects.

Unexpectedly, GFP-LC3 puncta were detected at late stages of L-Pro-induced esMT (days 3–5), frequently generating typical carousel-like structures (Supplementary Figures 4e and f). Indeed, toluidine blue or LysoTracker Red staining revealed prominent round acidic metachromatic vesicles (2–5 μ m in diameter) (Figure 4e) that resemble the autophagolysosomes that result from the fusion of early autophagosomes with lysosomes.²⁶ To assess their structure, 5-day-old ESC and PiC colonies were fixed, harvested, embedded in epoxy resin and sectioned (Figure 4f). According to their different phenotypes, thick (2 μ m) sections showed either strong or poor cell–cell adhesion contacts in ESC and PiC colonies, respectively (Figure 4f, *left panels*). Moreover, transmission electron microscopy (TEM) analysis of ultrathin sections (60 nm) confirmed the presence of large autophagolysosomes (~5 μ m in diameter) delimited by a double

membrane, with a typical narrow empty (electron-lucent) space between the two sheets (Figure 4f, *right panels*) and engulfing partially disintegrated organelles (including ER and mitochondria). Under TEM, we also observed multivesicular structures containing organelles, membrane cisternae and multilamellar bodies (Supplementary Figure 4g). We thus concluded that macroautophagy is induced during the late phases of the esMT (day 3 onwards), corresponding to the appearance of the ESC to PiC phenotypic transition.

***Atf4* downregulation promotes L-Pro-induced apoptosis in the EsMT.** Autophagy can protect cells against death, but it can also mediate cellular mortality under certain circumstances.²⁷ Interestingly, the presence of floating dead cells (Figure 5a), the detection of cell fragmentation/disintegration events by time-lapse microscopy (Figure 5b) and the increased number of apoptotic nuclei (Figure 5c) led us to hypothesise that apoptosis was induced during the esMT. Aside from morphological features, distinct hallmarks of apoptosis supported our hypothesis: loss of membrane integrity and asymmetry (Supplementary Figure 5a), caspase activity (Supplementary Figure 5b) and DNA fragmentation (Figures 5d and e; Supplementary Figure 5c). We thus concluded that the L-Pro-induced esMT is accompanied by massive apoptosis. Interestingly, although AAR activation promotes tumour-cell survival, *Atf4* downregulation induces apoptosis in cancer cells.²⁸ We thus reasoned that the L-Pro-dependent downregulation of *Atf4* (Figures 1 and 3) could at least partly explain apoptosis during the esMT. Consistent with our hypothesis, apoptotic DNA fragmentation significantly increased in L-Pro-treated *Atf4* KD ESCs compared with control (Supplementary Figure 5d, *left panel*). Moreover, *Atf4* overexpression counteracted the pro-apoptotic effect but not the pro-proliferative effect of L-Pro, and reduced autophagy in esMT (Figure 3i and Supplementary Figure 5d, *right panel*, and Supplementary Figure 5e). Therefore, we assessed the functional relevance of these findings by blocking apoptosis pharmacologically. The pan-caspase inhibitor Z-VAD reduced DNA fragmentation and further increased the survival of L-Pro-treated cells (Figures 5f–h). Remarkably, L-Pro/Z-VAD-treated ESCs generated flat colonies, which showed tight cell–cell contacts rather than the crown of mesenchymal-like cells typical of control colonies (Supplementary Figure 5f). Accordingly, cell migration was significantly impaired in L-Pro/Z-VAD-treated cells and was comparable to that of control ESCs (Figure 5i), suggesting that L-Pro-induced apoptosis is crucial for the acquisition of the motile mesenchymal-like phenotype. Interestingly, either Vitamin C⁴ or 2i (PD0325901/CHIR99021) inhibitors²⁹ counteracted the L-Pro-induced esMT (Supplementary Figure 5g), blocked DNA fragmentation (Supplementary Figure 5h) and increased cell survival (Supplementary Figure 5i). Together, our data provide evidence of a functional link between L-Pro-mediated *Atf4* downregulation and the acquisition of the motile mesenchymal-like phenotype in the esMT, which is accompanied by apoptosis induction (Figure 6).

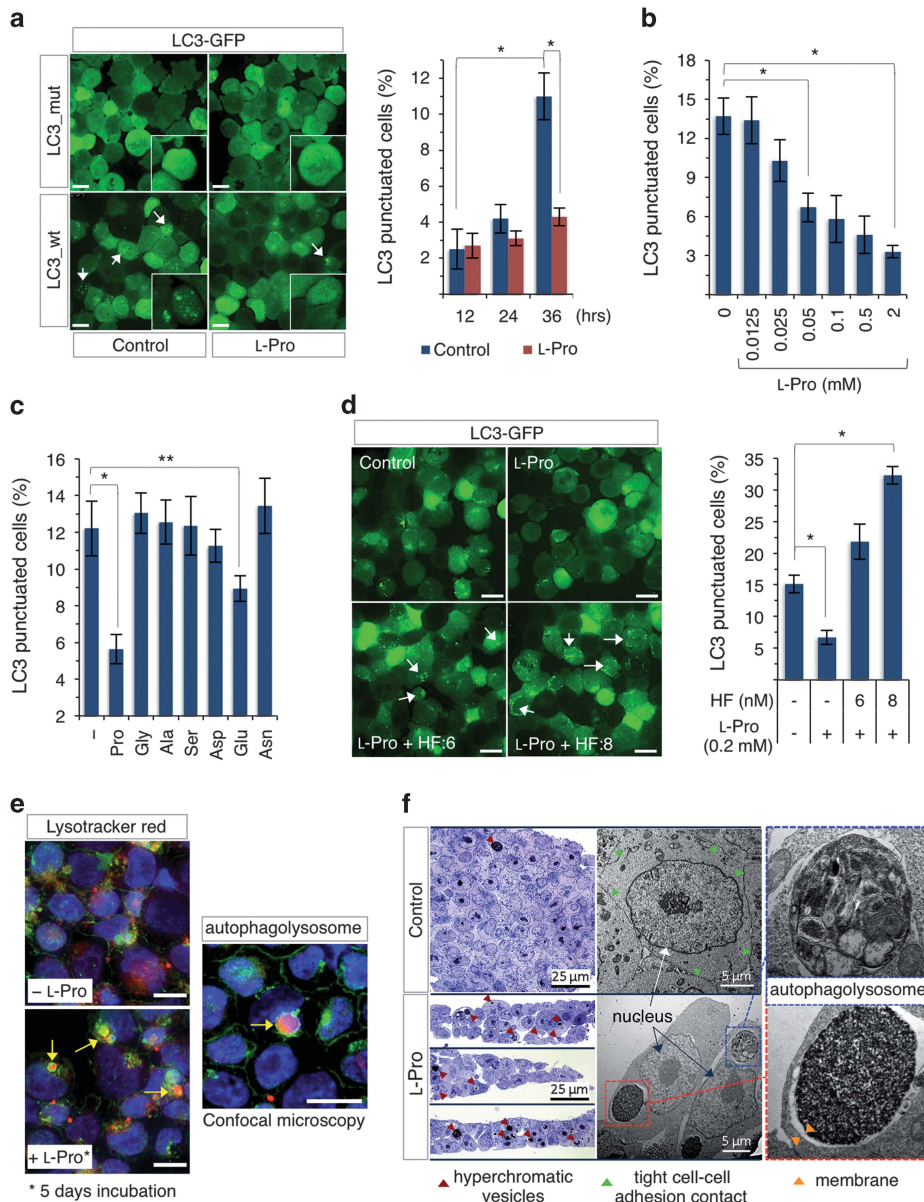


Figure 4 L-Pro regulates autophagy in ESCs and is counteracted by HF. **(a)** Time-course analysis of LC3 puncta formation in ESCs. Representative fluorescent photomicrographs (*left panel*) of LC3-GFP wild-type (LC3_wt) or GFP-LC3G120A mutant (LC3_mut) ESCs plated on gelatin +/- L-Pro (0.2 mM). Scale bar, 25 μ m. The number of cells with punctate LC3-GFP (*right panel*) was measured as the percentage (~400 cell scored/condition) of the total number of cells. **(b)** and **(c)** L-Pro supplementation prevents LC3-GFP re-localisation in a specific and dose-dependent manner. Punctate LC3-GFP ESCs were quantified after 36 h of treatment with increasing L-Pro concentrations **(b)** or with NEAAs **(c)**. **(d)** Representative fluorescent photomicrographs (*left panels*) of LC3-GFP localisation in control and ESCs treated with L-Pro (0.2 mM) either alone or with HF (6 and 8 nM). The quantification was performed 36 h after plating (*right panel*). **(e)** Representative microphotographs of acidic vesicular organelles (AVO) stained with toluidine blue dye (*left panels*, red arrows) and red-fluorescent acidic dye (LysoTracker Red, *right panels*, yellow arrows) in control (- L-Pro; *upper panel*) and L-Pro (0.2 mM; *lower panel*)-treated ESCs at day 5 of the esMT. Representative confocal image of autophagolysosomes. Scale bar, 25 μ m. **(f)** Transmission electron microscopy (TEM) analysis of control and L-Pro (0.2 mM)-treated ESCs at day 5 after plating. Representative images of the electron-dense bodies delimited by the double membrane, with a typical narrow empty (electron lucent) space between the two sheets (orange arrowheads). Data represent the mean \pm S.D. from **(a, b, c, and d)** three independent experiments, * $P < 0.001$, ** $P < 0.05$

Discussion

Pluripotent stem cells share the tendency to self-renew *in vitro* as tightly compacted cell aggregates (domed- or spherical-shaped colonies), thus recapitulating their *in vivo* behaviour.^{30,31} Here, we show that in mouse ESCs this phenotypic feature depends on a highly specific and controlled

shortage of the amino acid L-Proline (L-Pro). Indeed, ESCs although cultured in complete rich medium (DMEM/FBS/LIF) experience a specific L-Pro starvation. However, this intrinsic L-Pro shortage is not as extreme as to compromise ESC survival, but it is sufficient to limit their proliferation and influence the gene expression profile. In most cell lines, including ESCs, a condition of amino-acid limitation leads to

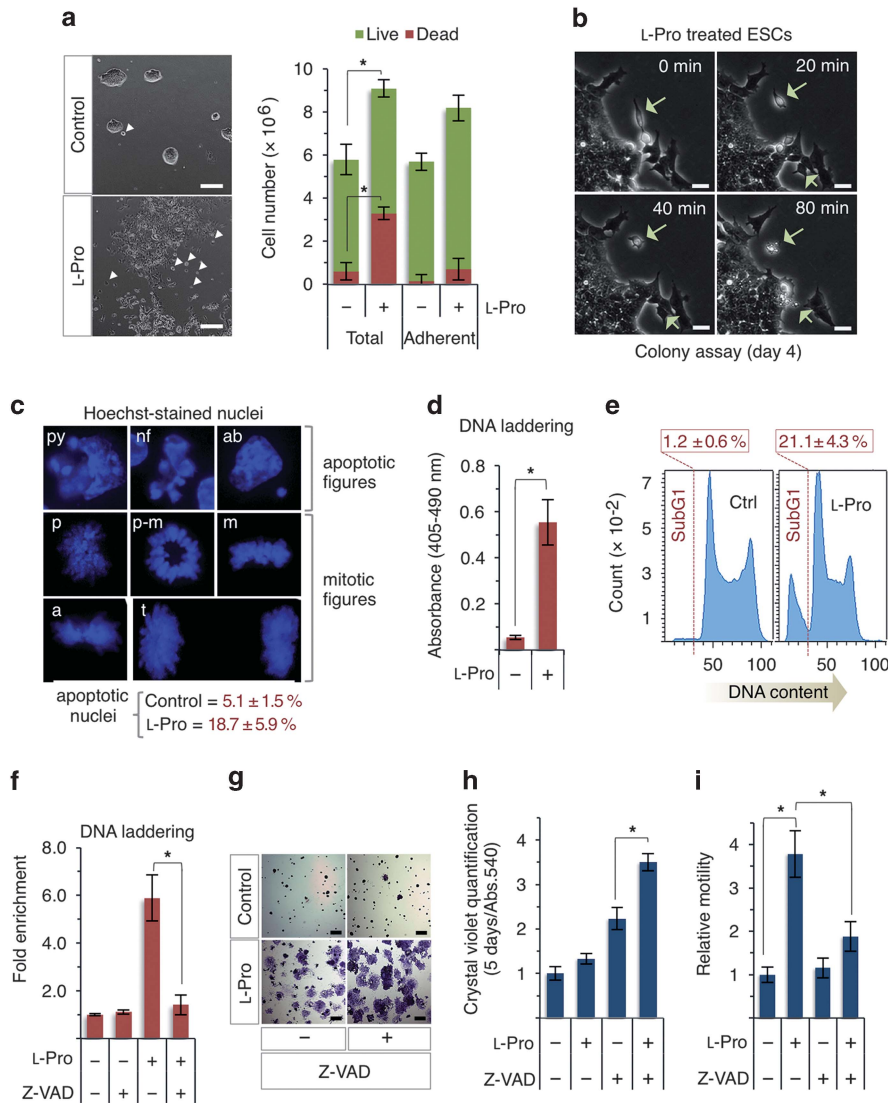


Figure 5 Apoptotic cell death occurs during L-Pro-induced esMT. (a) Representative photomicrographs of control and L-Pro (0.5 mM)-treated ESCs at day 5 after plating (*left panel*). Arrowheads indicate floating cells and debris. Scale bar, 100 μ m. Quantification of dead cells by the trypan blue exclusion assay (*right panel*) in adherent and total (floating plus adherent) cell populations. (b) Representative frames of time-lapse series of L-Pro-treated ESCs. Arrowheads indicate cells located at the periphery of a flat colony exploding into a cascade of apoptotic-like bodies. Scale bar, 25 μ m. (c) Representative fluorescent photomicrographs of Hoechst-stained nuclei. Apoptotic figures, including a pyknotic nucleus (py), nuclear fragmentation (nf) and apoptotic bodies (ab), were distinguished from mitotic figures, prophase (p), pro-metaphase (p-m), metaphase (m), anaphase (a) and telophase (t). Data show the percentage of apoptotic nuclei (~900 nuclei scored/condition) in control and L-Pro-treated ESC cultures (day 5). (d) Quantitative determination of DNA laddering by a photometric immunoassay. (e) FACS analysis of Propidium Iodide (PI)-stained control or L-Pro-treated ESCs. The fraction of cells in SubG1 phase is indicated. (f–h) Effect of Z-VAD on L-Pro-induced esMT and cell motility. Quantitative analysis of DNA fragmentation (f) in control or L-Pro (0.2 mM)-treated ESCs either alone or in the presence of Z-VAD (0.1 mM). Representative photomicrographs of the colonies (g) showing round (ESC) or flat (PiC) phenotype. Scale bar, 200 μ m. (h) Quantification of crystal violet staining of cell colonies generated in the different culture conditions. Effect of Z-VAD on cell motility (i). ESCs were treated with L-Pro +/- Z-VAD for 5 days or left untreated as a control, and cell migration was assessed and expressed as the average number of cells migrating towards an FBS gradient (1–15%). Data represent the mean \pm S.D. from (c, d, e, f and i) three or (h) five independent experiments, * $P < 0.001$

the induction of the amino-acid starvation response (AAR/Atf4) pathway and autophagy^{10,25,32} and, if protracted and uncompensated, this condition leads to apoptotic cell death. Accordingly, AAR and autophagy, but not apoptosis, are progressively induced in feeder-free growing ESCs and are specifically counteracted by exogenously added L-Pro in a dose-dependent manner. Moreover, L-Pro starvation exerts similar effects to that of pharmacological-induced starvation of an essential amino acid (EAA), such as Histidine (L-His).²⁵ It is known that EAAs cannot be synthesised by the cells and must

be exogenously provided; conversely, NEAAs, such as L-Pro, can be produced by the cells, either *de novo* or from other amino acids.³³ Thus, the finding that an intrinsic limitation of L-Pro occurs in ESCs cultured in complete rich medium was totally unexpected. Interestingly, although it was not specifically discussed, a previous report showed that only the deprivation of L-Pro among all the NEAAs limits the *in vitro* colony formation ability of E14Tg2A ESCs.² Of note, mouse fibroblasts release L-Pro,³⁴ which likely explain why feeder cells protect ESCs from this nutrient starvation response.

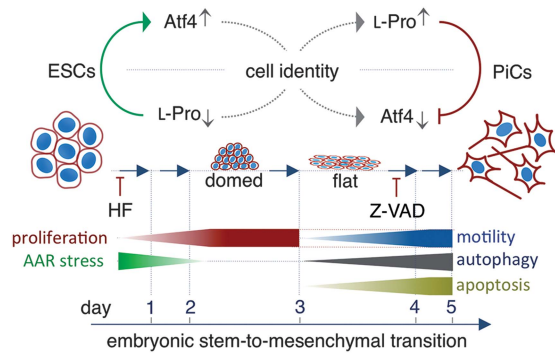


Figure 6 Model depicting the role of L-Pro ↔ AAR axis in the control of stem cell identity. The ESC identity depends on a highly specific intrinsic nutrient stress condition generated by a L-Pro-AAR/Atf4 axis. Under L-Pro shortage/AAR activation condition, ESCs grow as a compact, adherent cell mass (i.e., like the inner cell mass in the blastocyst). Alleviation of this stress (L-Pro fullness/AAR inactivation) initially improves ESC proliferation, but later on it induces the esMT, which is accompanied by a huge induction of macroautophagy and apoptosis. During the esMT, ESCs acquire mesenchymal-like features, becoming highly motile and invasive pluripotent stem cells. Targeting of the L-Pro ↔ AAR/Atf4 axis genetically (*Atf4* LOF and GOF approaches) or pharmacologically (HF, Z-VAD) modulates esMT

How L-Pro shortage stress is generated in ESCs? L-Pro is unique among the NEAAs because, due to its atypical cyclic (pyrrolidine ring) structure it is synthesised by highly specific enzymes encoded by *Aldh18a1* and *Pycr1* genes.³⁵ The generation of *Atf4* GOF and LOF cell lines allowed us to identify a L-Pro-AAR/Atf4-*Aldh18a1*/*Pycr1* autoregulatory loop in ESCs. Indeed, upon *Atf4* overexpression *Aldh18a1*/*Pycr1* expression increases and ESCs are less dependent on exogenous L-Pro; conversely, *Atf4* knockdown reduces *Aldh18a1*/*Pycr1* expression and increases ESC requirement for L-Pro to proliferate. Thus, by placing the expression of L-Pro biosynthesis genes (*Aldh18a1* and *Pycr1*) under the control of AAR/Atf4, and AAR/Atf4 under the control of L-Pro availability, this loop maintains L-Pro as a growth limiting metabolite in ESCs. Notably, L-Glu and L-Orn, two metabolic precursors of L-Pro, when added to the culture medium are less efficient than L-Pro in (i) inactivating the AAR and (ii) inducing ESC proliferation, thus supporting the idea that L-Pro biosynthesis is reduced/inefficient in ESCs. This finely tuned interplay between AAR/Atf4 and L-Pro biosynthetic pathway might be relevant also in other biological processes. Actually, while *Gcn2* is dispensable for mouse embryogenesis,³⁶ *Atf4* is critical for the proper differentiation and function of osteoblasts³⁷ and chondroblasts,³⁸ which are characterised by a marked ability to synthesise and secrete the L-Pro-rich protein collagens. The *Atf4* ↔ L-Pro functional axis may thus explain the skeletal abnormalities of *Atf4* knockout mice,³⁷ and it suggests that they may be at least partially rescued by increased L-Pro intake.

Why should a L-Pro starvation condition be maintained in ESCs? Several evidence indicate that this condition is required to preserve ESC morphological and molecular identity. Indeed, in line with the assumption that L-Pro is a limiting factor in ESCs, addition of L-Pro rapidly inactivates AAR pathway, reduces autophagy and improves ESC proliferation. Nevertheless, if this optimal growth condition (L-Pro fullness/AAR inactive) is protracted in time (48–72 h),

then ESCs progressively lose their ability to grow as domed-like colonies maintaining tight cell–cell adhesion contacts, and undergo esMT becoming mesenchymal-like, free motile, pluripotent stem cells. The molecular mechanism(s) underlying the complex/multiphase esMT process are still far to be fully elucidated. However, here we demonstrate that a selective inhibitor of the prolyl-tRNA synthetase (PRS, L-Pro-tRNA loading),^{14,15} that is, Halofuginone (HF, L-Pro-tRNA loading),^{14,15} that is, Halofuginone (HF), avoids L-Pro-induced esMT and preserves ESC identity. The fact that supplemental L-Pro requires an efficient prolyl-tRNA synthetase to modify ESC behaviour further supports the idea that ESCs experience a specific L-Pro shortage and that L-Pro inactivates the AAR stress by reducing the levels of unloaded tRNAs, that is, of the AAR inducer. Accordingly, L-Pro addition induces the expression of type I collagen in ESCs (data not shown). Collagens are L-Pro-rich proteins whose synthesis is highly dependent on L-Pro-tRNA, and it has been shown that HF prevents collagens accumulation/fibrosis in muscular dystrophies.³⁹ Furthermore, one of the most rapidly induced gene in response to L-Pro is *Lefty1*, and its expression is counteracted by HF. Interestingly, *Lefty* is an inhibitor of TGFβ, which is a well-known inducer of EMT, and a regulator of collagen homeostasis.⁷ Finally, Vitamin C (VitC),⁴⁰ which is a potent antagonist of L-Pro-induced esMT,^{1,4} is a well-known regulator of collagens homeostasis. Indeed, nascent collagens are modified by the VitC-dependent proline dioxygenases at the level of endoplasmic reticulum (ER), and it has been reported that ER stress is signalled through the protein kinase RNA-like endoplasmic reticulum kinase (Perk)-Eif2α-Atf4 pathway to maintain the pool of haematopoietic stem cells.⁴¹ Thus, we suggest that a functional link between Atf4 stress signalling and L-Pro availability/collagens homeostasis may be relevant for esMT and EMT, which is a key event in development, tumour progression and fibrosis.^{8,42}

Our findings that the late phases of esMT are accompanied by macroautophagy and massive apoptotic cell death highlight an apparent paradox. In fact, autophagy occurs in ESCs cultured without supplemental L-Pro (AAR active/Atf4 high), as well as during esMT, that is, when ESCs are cultured with supplemental L-Pro (AAR inactive/Atf4 low). Supplemental Glycine, Asparagine or a mix of NEAAs do not block autophagy and apoptosis (data not shown), thus excluding a role of amino-acid starvation. Of note, it has been reported that imbalanced expression of the stress-activated transcription factor Atf4 (either increase or decrease) may lead to autophagy and apoptosis in different cell types.^{10,28} Our findings are in line with this idea; indeed, forced *Atf4* expression prevents L-Pro-induced acquisition of the motile phenotype and reduces autophagy and apoptosis. In conclusion, here we provide the first evidence that mouse ESC identity depends on the finely tuned regulation of L-Pro biosynthesis by the AAR/Atf4 pathway (Figure 6), and provide novel insights into the emerging role of the stress response in reprogramming cell identity.⁴³

Materials and Methods

ESC culture, treatments and differentiation. Wild-type TBV2 (129/SvP) and E14Tg2 (E14) mouse ESCs were maintained on a feeder layer of mitomycin C-treated MEFs and on feeder-free gelatin-coated plates, respectively, according to standard procedures. PICs were generated as previously described.¹⁴

Briefly, ESCs were seeded at low density (50–500 cells/cm²) onto gelatin-coated plates and grown in the presence of L-Pro (500 μM–1 mM) for 5 days. Medium was changed at day 3 with addition of fresh L-Pro. PiCs were harvested using accutase (Sigma-Aldrich, St. Louis, MO, USA) and cultured in the presence of L-Proline (500 μM). Both ESCs and PiCs were cultured in high glucose Dulbecco's modified Eagle's medium (Invitrogen, Life Technologies, Eugene, OR, USA) supplemented with 15% ES-screened fetal bovine serum (FBS, Euroclone, Milan, Italy), 0.1 mM β-mercaptoethanol (Sigma-Aldrich), 1 mM sodium pyruvate, 2 mM glutamine, 100 U/ml penicillin/streptomycin all from GIBCO (Carlsbad, CA, USA) and 1000 U/ml recombinant LIF (ESGRO, Millipore, Darmstadt, Germany).

For Halofuginone (HF) treatments, HF (Sigma-Aldrich) was dissolved in DMSO (2 mM) and used at the indicated concentrations (1–20 nM). Amino acids including L-Pro, NEAAs (L-Gly, L-Ala, L-Ser, L-Asp, L-Glu and L-Asn) and L-Orn were purchased from Sigma-Aldrich. Cycloheximide, Histidinol, NAC and GSH (Sigma-Aldrich) were dissolved in water and used at the indicated concentrations (0.15–0.6 μg/ml; 0.6–2.4 mM, 0.625–5 mM and 0.04–5 mM, respectively).

For cardiac differentiation, ESCs were induced to form embryoid bodies (EBs) in hanging drops (500 cells/drop) and were further differentiated without addition of growth factors, as described.⁴⁴ Neuronal differentiation was performed as previously described.⁴⁵

Generation of *Atf4* KD and GOF ES cell lines. To generate *Atf4* KD ESCs, 1 × 10⁶ undifferentiated TBV2 ESCs were infected with either non-targeting control or *Atf4* shRNA lentiviruses (pLKO.1 vectors, Open Biosystems, GE Dharmacon, Lafayette, CO, USA). Twenty-four hours after infection, cells were subjected to puromycin selection (Sigma-Aldrich, 2 μg/ml) for 2 days and subsequently grown for additional 4–5 days, until clones appeared. Clones were pulled together and silencing efficacy was evaluated at RNA and protein levels. Four independent shRNA viral vectors, targeting different *Atf4* mRNA sequences, were used and one shRNA vector was selected on the basis of the highest silencing efficacy.

Atf4 Tet-Off ESCs (*Atf4* GOF) were generated as previously described.⁴⁶ Briefly, mouse *Atf4* cDNA (OriGene; cat. n. MR29597) was cloned in the exchange vector pPTHC/MCS⁴⁷ and then targeted to the Rosa26 locus of the EB3 ESCs, as described.¹⁹ A PCR-based assay on genomic DNA was used to identify the positive clones.¹⁹ Two independent clones were tested for *Atf4* mRNA and protein induction upon tetracycline (Sigma-Aldrich, 1 μg/ml) removal.

L-Pro measurement. The intracellular concentration of free L-Proline in ESCs, PiCs and mouse embryonic fibroblasts (MEFs) was quantified as previously described.⁴⁸

Colony assay, alkaline phosphatase and crystal violet staining. For colony phenotype assay, ESCs were plated at low density (50–250 cells/cm²) in complete medium (DMEM/15%FBS/LIF) on gelatin-coated plates and colonies were grown for 5 days in the presence/absence of L-Pro (250–500 μM), with a medium change at day 3.

Alkaline phosphatase activity was assessed using the AP staining kit (System Biosciences, Mountain View, CA, USA), following the manufacturer's instructions.

Staining with crystal violet was performed as previously described.¹ Briefly, cells were washed twice with phosphate-buffered saline (PBS) and fixed/stained with a solution of 6% glutaraldehyde and crystal violet. After 30 min at RT, cells were carefully washed with tap water and dried for further analysis. For quantification, crystal violet was dissolved with 30% acetic acid (1 ml) for 15 min at RT and absorbance was read at 540 nm, using the Synergy H1 Microplate Reader (BioTek, Winooski, VT, USA).

Proliferation assays and viable cell count. For the cell proliferation assay, ESCs were plated at 1.5 × 10⁴ cells/cm² on gelatin-coated plates in ESC medium with or without L-Pro and cell viability was measured at 36 h, using the colorimetric CyQuant[®] cell proliferation assay (Invitrogen), following the manufacturer's instructions. Briefly, triplicate samples were washed with PBS and stored at –80 °C for 2 h. After thawing, cells were incubated with a mix of cell lysis buffer and CyQUANT-GR dye. Absorbance was analysed at 480–520 nm, using the Fluoroskan Ascent FL Microplate Fluorometer and Luminometer (Thermo Fisher Scientific, Waltham, MA, USA).

For the proliferation assay, the Click-iT EdU Flow Cytometry Assay (Invitrogen) was used. Briefly, cells were incubated with 5-ethynyl-2'-deoxyuridine (EdU) (10 μM; overnight at 37 °C), dissociated, fixed and permeabilized, following the manufacturer's instructions. Samples were analysed at FACS-Canto using the DivaTM software (BD Biosciences, San Jose, CA, USA).

Viable count was performed on triplicate samples; briefly, cells were counted on the Cellometer Auto T4 (Nexcelom Bioscience, Lawrence, MA, USA) and % viability was simultaneously calculated by trypan blue exclusion.

Cell migration. Migration assays were performed using polycarbonate (5 μm pore, Costar, Tewksbury, MA, USA) or PET membrane transwells (8 μm pore; BD Biosciences). Cells were detached with accutase (Sigma-Aldrich) plated (2 × 10⁴/transwell) and incubated for 20–22 h as previously described.⁴

Time lapse experiments. ESCs were seeded on gelatin-coated plates at 50 cells/cm² and grown in complete medium supplemented with appropriate compounds. Images were captured (×20) every 5 min for 24 h using a Leica DMI6000B inverted microscope equipped with a microscope incubator (Okolab, Naples, Italy).

Real-time PCR. Total RNAs were isolated using RNeasy mini kit (Qiagen, Hilden, Germany) and retro-transcribed using the QuantiTect Reverse Transcription kit (Qiagen). SYBR Green PCR master mix (FluoCycle II SYBR, Euroclone) was used for quantitative real-time PCR. Primers are in Supplementary Table 2. For microarray experiments, RNA samples were analysed at the microarray facility of the Ohio State University as previously described.⁴ Statistical data analysis was performed at the Bioinformatics Core Facility (<http://bioinformatics.tigem.it>) of TIGEM, Italy. The relative signal intensities of each probe across the six samples assayed for each cell line were evaluated selecting a false discovery rate (FDR) of < 0.001 to assess significant gene differential expressions. Genes were classified based on Gene Ontology terms (DAVID Bioinformatics Resources; <http://david.abcc.ncifcrf.gov>).

Immunoblotting. Whole-cell lysates were prepared either in 20 mM Tris pH 7.9, 120 mM KCl, 5 mM MgCl₂, 0.2% Nonidet P-40, 5 mM EDTA, 10% glycerol (for PARP1 and Casp3 analysis) or in 100 mM Tris pH 8, 140 mM NaCl, 20 mM EDTA, 0.2% SDS, 1% Nonidet P-40 lysis buffer, resolved on SDS-PAGE gels and transferred onto PVDF membranes using the iBlot dry Transfer System (Life Technologies, Carlsbad, CA, USA). Blocked membranes were incubated with the following primary antibodies: Atf-4 (1 : 500); eIF2α (1 : 1000); phospho-eIF2α (1 : 500); PARP1 (1 : 1000, Cell Signaling Technology, CST, Danvers, MA, USA), which detects the full-length protein (116 kDa) as well as the large caspase-cleaved fragment (89 kDa); anti-Casp3 (1 : 1000) all from CST, and anti-LC3 (2 μg/ml, Novus Biologicals, Littleton, CO, USA) anti-Gapdh (1 : 10 000, Abcam, Cambridge, UK), followed by the appropriate HRP-conjugated secondary antibodies (1 : 10000, Dako, Glostrup, Denmark). Detection was performed with ECL reagents (Pierce, Thermo Scientific, Waltham, MA, USA). The ImageJ software (open source; <http://imagej.nih.gov/ij>) was used for densitometric quantification.

Preparation of cytospin samples. Cells (1–1.5 × 10⁴) were dissociated with accutase for 5 min at 37 °C and resuspended in 15% FBS/1x PBS. Cell samples were centrifuged at 900 r.p.m. for 15 min onto glass slides (2 spots of 1 × 10⁵ cells each) using a Thermo Shandon Cytocentrifuge (CytoSpin 4, Thermo Fisher Scientific). Specimens were directly analysed or fixed for further analysis.

Immunofluorescence analysis. Differentiated EBs and monolayer cultures were fixed with 4% paraformaldehyde (PFA) and permeabilized with 0.1% Triton X-100 at RT. The following primary antibodies were used: MF20 (1 : 50, Developmental Studies Hybridoma Bank); βIII Tubulin (1 : 400, Sigma-Aldrich). After washing in 0.5% Tween-1 × PBS, cells were incubated with secondary antibodies (1 : 200, Alexa Fluor, Molecular Probes Inc., Life Technologies).

For autophagy detection, cytospin samples (see above) were stained with LysoTracker Red DND-99 dye. Briefly, cells (50 000 cells/spot) were washed with PBS 1 ×, stained with LysoTracker Red DND-99 dye (Molecular Probes Inc.) for 1 min at room temperature. Cells were gently washed and fixed in 4% PFA for 30 min, washed three times with PBS, and stained with membrane stain WGA-Alexa Fluor 488 Conjugate (Invitrogen) following the manufacturer's instructions. Cell nuclei were counterstained with Hoechst 33342 (Invitrogen). Images were obtained using the DMI6000B microscope and the DFC 350FX B/W digital camera (Leica, Solms, Germany). Leica FW4000 and AF6000 software were used for image acquisition/elaboration. Confocal images were acquired at ×63 magnification on a LSM710 confocal fluorescence microscope (Carl Zeiss Inc., Jena, Germany) using the ZEN 2008 software (Carl Zeiss Inc.).

Toluidine blue staining. Samples were fixed with 4% PFA, washed three times with PBS and stained with toluidine blue (1% in water) for 10 min at RT. The samples were observed using a DM6000B upright microscope and the LAS V 4.0 software (Leica) was used for images acquisition.

Nuclear morphology analysis. Cells (floating and adherent) were cytospinned (see above), fixed in 4% PFA and the nuclei were stained with Hoechst 33342 (Invitrogen) in 1 × PBS with 0.1% Triton X-100. Fluorescent labelling was visualised using the DM6000B microscope (Leica) and images acquired with the DFC 350FX B/W camera.

Apoptosis assays. DNA laddering associated with apoptotic cell death was quantified by spectrophotometric detection of cleaved DNA/histone complexes, using the Cell Death Detection ElisaPlus kit (Roche, Welwyn Garden City, UK), following the manufacturer's instructions. The immunoassay was performed on duplicate samples by measuring at 405 nm against a blank solution (with a 490-nm reference wavelength).

For subG1 determination, floating and adherent sub-populations (at day 5) were collected, permeabilized and stained in 0.1% Na citrate, 0.1% Triton X-100, 0.2 μg/ml propidium iodide (PI), 50 μg/ml DNase-free RNase.

For detection of membrane asymmetry, intact cells were labelled with Alexa Fluor 488 Annexin V and PI using the Dead Cell Apoptosis Kit (Invitrogen) following the manufacturer's instructions. Samples were analysed at FACS-Canto using the DivaTM software (BD Biosciences).

Transmission electron microscopy. Cells (ESCs and PiCs) were fixed in 2.5% glutaraldehyde in cacodylate buffer, post-fixed in osmium tetroxide, dehydrated, and embedded in Epon 812 (PolyScience, Warrington, PA, USA). Ultrathin (60 nm) sections were cut on a Leica ultracut UCT ultramicrotome (Leica Microsystems) and contrasted with uranyl acetate and lead citrate. Grids were examined using a Jeol JEM-1011 (Jeol, Tokyo, Japan) transmission electron microscope (TEM) (100 kV, high contrast and brightness with optimum resolution) and micrographs were taken with iTEM software (Olympus Soft Imaging System, Münster, Germany).

Statistical analysis. Statistical significance was determined by a two-tailed paired Student's *t*-test. *P*-values < 0.01 were considered as statistically significant. Error bars show mean ± S.D. unless otherwise indicated.

Conflict of Interest

The authors declare no conflict of interest.

Acknowledgements. We thank the Animal House, the Integrated Microscopy and the FACS Facilities of IGB-CNR. We also thank Annamaria Carissimo and the Bioinformatics Core Facility of Telethon Institute of Genetics and Medicine (TIGEM). We thank Stefania Comes and Nicola Laprano for having started this project, and Antonietta Coppola and Gennaro Andolfi for technical assistance. We are grateful to Maurizio Iaccarino and Antonio Baldini for helpful discussions. This work is supported by AIRC (grant 11599), the European Community's Seventh Framework Programme ENDOSTEM (no. 241440), the Epigenomics Flagship Project (EPIGEN) of the MIUR-CNR, the Italian Ministry of Education-University-Research (MIUR-PRIN and PON Cluster IRMI) to GM. EJP is supported by a grant from Medical Research in Italy (RBNE08HM7T-003).

- Casalino L, Comes S, Lambazzi G, De Stefano B, Filosa S, De Falco S *et al*. Control of embryonic stem cell metastability by L-proline catabolism. *J Mol Cell Biol* 2011; **3**: 108–122.
- Wang J, Alexander P, Wu L, Hammer R, Cleaver O, McKnight SL. Dependence of mouse embryonic stem cells on threonine catabolism. *Science* 2009; **325**: 435–439.
- Shyh-Chang N, Locasale JW, Lysiotis CA, Zheng Y, Teo RY, Ratanasiriintraoat S *et al*. Influence of threonine metabolism on S-adenosylmethionine and histone methylation. *Science* 2013; **339**: 222–226.
- Comes S, Gagliardi M, Laprano N, Fico A, Cimmino A, Palamidessi A *et al*. L-proline induces a mesenchymal-like invasive program in embryonic stem cells by remodeling H3K9 and H3K36 methylation. *Stem Cell Reports* 2013; **1**: 307–321.
- Shiraki N, Shiraki Y, Tsuyama T, Obata F, Miura M, Nagae G *et al*. Methionine metabolism regulates maintenance and differentiation of human pluripotent stem cells. *Cell Metab* 2014; **19**: 780–794.
- Nieto MA. The ins and outs of the epithelial to mesenchymal transition in health and disease. *Annu Rev Cell Dev Biol* 2011; **27**: 347–376.
- Lamouille S, Xu J, Derynck R. Molecular mechanisms of epithelial-mesenchymal transition. *Nat Rev Mol Cell Biol* 2014; **15**: 178–196.
- Nieto MA. Epithelial plasticity: a common theme in embryonic and cancer cells. *Science* 2013; **342**: 1234850.
- Ohnishi Y, Huber W, Tsumura A, Kang M, Xenopoulos P, Kurimoto K *et al*. Cell-to-cell expression variability followed by signal reinforcement progressively segregates early mouse lineages. *Nat Cell Biol* 2014; **16**: 27–37.
- Han J, Back SH, Hur J, Lin YH, Gildersleeve R, Shan J *et al*. ER-stress-induced transcriptional regulation increases protein synthesis leading to cell death. *Nat Cell Biol* 2013; **15**: 481–490.
- Wek RC, Ramirez M, Jackson BM, Hinnebusch AG. Identification of positive-acting domains in GCN2 protein kinase required for translational activation of GCN4 expression. *Mol Cell Biol* 1990; **10**: 2820–2831.
- Zaborske JM, Narasimhan J, Jiang L, Wek SA, Dittmar KA, Freimoser F *et al*. Genome-wide analysis of tRNA charging and activation of the eIF2 kinase Gcn2p. *J Biol Chem* 2009; **284**: 25254–25267.
- Harding HP, Zhang Y, Zeng H, Novoa I, Lu PD, Calton M *et al*. An integrated stress response regulates amino acid metabolism and resistance to oxidative stress. *Mol Cell* 2003; **11**: 619–633.
- Keller TL, Zocco D, Sundrud MS, Hendrick M, Edenius M, Yum J *et al*. Halofuginone and other febrifugine derivatives inhibit prolyl-tRNA synthetase. *Nat Chem Biol* 2012; **8**: 311–317.
- Zhou H, Sun L, Yang XL, Schimmel P. ATP-directed capture of bioactive herbal-based medicine on human tRNA synthetase. *Nature* 2013; **494**: 121–124.
- Phang JM, Donald SP, Pandhare J, Liu Y. The metabolism of proline, a stress substrate, modulates carcinogenic pathways. *Amino Acids* 2008; **35**: 681–690.
- Lettieri Barbato D, Aquilano K, Baldelli S, Cannata SM, Bernardini S, Rotilio G *et al*. Proline oxidase-adipose triglyceride lipase pathway restrains adipose cell death and tissue inflammation. *Cell Death Differ* 2014; **21**: 113–123.
- Washington JM, Rathjen J, Felquer F, Lonic A, Bettess MD, Hamra N *et al*. L-Proline induces differentiation of ES cells: a novel role for an amino acid in the regulation of pluripotent cells in culture. *Am J Physiol Cell Physiol* 2010; **298**: C982–C992.
- De Cegli R, Romito A, Iacobacci S, Mao L, Lauria M, Fedele AO *et al*. A mouse embryonic stem cell bank for inducible overexpression of human chromosome 21 genes. *Genome Biol* 2010; **11**: R64.
- Deval C, Chaveroux C, Maurin AC, Cherasse Y, Parry L, Carraro V *et al*. Amino acid limitation regulates the expression of genes involved in several specific biological processes through GCN2-dependent and GCN2-independent pathways. *FEBS J* 2009; **276**: 707–718.
- Mizushima N, Levine B, Cuervo AM, Klionsky DJ. Autophagy fights disease through cellular self-digestion. *Nature* 2008; **451**: 1069–1075.
- Levine B, Kroemer G. Autophagy in the pathogenesis of disease. *Cell* 2008; **132**: 27–42.
- Kabeaya Y, Mizushima N, Ueno T, Yamamoto A, Kirisako T, Noda T *et al*. LC3, a mammalian homologue of yeast Apg8p, is localized in autophagosome membranes after processing. *EMBO J* 2000; **19**: 5720–5728.
- Guo Y, Chang C, Huang R, Liu B, Bao L, Liu W. AP1 is essential for generation of autophagosomes from the trans-Golgi network. *J Cell Sci* 2012; **125**: 1706–1715.
- Shan J, Hamazaki T, Tang TA, Terada N, Kilberg MS. Activation of the amino acid response modulates lineage specification during differentiation of murine embryonic stem cells. *Am J Physiol Endocrinol Metab* 2013; **305**: E325–E335.
- Xie Z, Klionsky DJ. Autophagosome formation: core machinery and adaptations. *Nat Cell Biol* 2007; **9**: 1102–1109.
- Mauri MC, Zalckvar E, Kimchi A, Kroemer G. Self-eating and self-killing: crosstalk between autophagy and apoptosis. *Nat Rev Mol Cell Biol* 2007; **8**: 741–752.
- Ye J, Kumanova M, Hart LS, Sloane K, Zhang H, De Panis DN *et al*. The GCN2-ATF4 pathway is critical for tumour cell survival and proliferation in response to nutrient deprivation. *EMBO J* 2010; **29**: 2082–2096.
- Ying QL, Wray J, Nichols J, Battle-Morera L, Doble B, Woodgett J *et al*. The ground state of embryonic stem cell self-renewal. *Nature* 2008; **453**: 519–523.
- Reynolds BA, Weiss S. Generation of neurons and astrocytes from isolated cells of the adult mammalian central nervous system. *Science* 1992; **255**: 1707–1710.
- Dontu G, Al-Hajj M, Abdallah WM, Clarke MF, Wicha MS. Stem cells in normal breast development and breast cancer. *Cell Prolif* 2003; **36**: 59–72.
- Shan J, Lopez MC, Baker HV, Kilberg MS. Expression profiling after activation of the amino acid deprivation response in HepG2 human hepatoma cells. *Physiol Genomics* 2010; **41**: 315–327.
- Wu G. Amino acids: metabolism, functions, and nutrition. *Amino acids* 2009; **37**: 1–17.
- Stoner GD, Merchant DJ. Amino acid utilization by L-M strain mouse cells in a chemically defined medium. *In vitro* 1972; **7**: 330–343.
- Phang JM, Liu W, Zabirnyk O. Proline metabolism and microenvironmental stress. *Annu Rev Nutr* 2010; **30**: 441–463.
- Zhang P, McGrath BC, Reinert J, Olsen DS, Lei L, Gill S *et al*. The GCN2 eIF2alpha kinase is required for adaptation to amino acid deprivation in mice. *Mol Cell Biol* 2002; **22**: 6681–6688.
- Yang X, Matsuda K, Bialek P, Jacquot S, Masuoka HC, Schinke T *et al*. ATF4 is a substrate of RSK2 and an essential regulator of osteoblast biology; implication for Coffin-Lowry Syndrome. *Cell* 2004; **117**: 387–398.

38. Wang W, Lian N, Li L, Moss HE, Wang W, Perrien DS *et al*. Atf4 regulates chondrocyte proliferation and differentiation during endochondral ossification by activating Ihh transcription. *Development* 2009; **136**: 4143–4153.
39. McLaughlin NP, Evans P, Pines M. The chemistry and biology of febrifugine and halofuginone. *Bioorg Med Chem* 2014; **22**: 1993–2004.
40. Du J, Cullen JJ, Buettner GR. Ascorbic acid: chemistry, biology and the treatment of cancer. *Biochim Biophys Acta* 2012; **1826**: 443–457.
41. van Galen P, Kreso A, Mbong N, Kent DG, Fitzmaurice T, Chambers JE *et al*. The unfolded protein response governs integrity of the haematopoietic stem-cell pool during stress. *Nature* 2014; **510**: 268–272.
42. Oskarsson T, Battle E, Massague J. Metastatic stem cells: sources, niches, and vital pathways. *Cell Stem Cell* 2014; **14**: 306–321.
43. Vilchez D, Simic MS, Dillin A. Proteostasis and aging of stem cells. *Trends Cell Biol* 2014; **24**: 161–170.
44. Parisi S, D'Andrea D, Lago CT, Adamson ED, Persico MG, Minchiotti G. Nodal-dependent Cripto signaling promotes cardiomyogenesis and redirects the neural fate of embryonic stem cells. *J Cell Biol* 2003; **163**: 303–314.
45. Fico A, Manganelli G, Simeone M, Guido S, Minchiotti G, Filosa S. High-throughput screening-compatible single-step protocol to differentiate embryonic stem cells in neurons. *Stem Cells Dev* 2008; **17**: 573–584.
46. D'Aniello C, Fiorenzano A, Iaconis S, Liguori GL, Andolfi G, Cobellis G *et al*. The G-protein-coupled receptor APJ is expressed in the second heart field and regulates Cerberus-Baf60c axis in embryonic stem cell cardiomyogenesis. *Cardiovasc Res* 2013; **100**: 95–104.
47. Masui S, Shimosato D, Toyooka Y, Yagi R, Takahashi K, Niwa H. An efficient system to establish multiple embryonic stem cell lines carrying an inducible expression unit. *Nucleic Acids Res* 2005; **33**: e43.
48. Liu W, Le A, Hancock C, Lane AN, Dang CV, Fan TW *et al*. Reprogramming of proline and glutamine metabolism contributes to the proliferative and metabolic responses regulated by oncogenic transcription factor c-MYC. *Proc Natl Acad Sci USA* 2012; **109**: 8983–8988.



This work is licensed under a Creative Commons Attribution-NonCommercial-NoDerivs 4.0 International License. The images or other third party material in this article are included in the article's Creative Commons license, unless indicated otherwise in the credit line; if the material is not included under the Creative Commons license, users will need to obtain permission from the license holder to reproduce the material. To view a copy of this license, visit <http://creativecommons.org/licenses/by-nc-nd/4.0/>

Supplementary Information accompanies this paper on Cell Death and Differentiation website (<http://www.nature.com/cdd>)